Towards Space-hardened, Small-lightweight Laser Range Imager for Planetary Exploration Rover

Genya Ishigami*, Takahide Mizuno**

*Dept. of Mechanical Engineering, Keio University, Japan
e-mail: ishigami@mech.keio.ac.jp

**Institute of Space and Astronautical Science, Japan Aerospace Exploration Agency, Japan
e-mail:tmizuno@isas.jaxa.jp

Abstract

Laser-based ranging techniques have been recently exploited for an application to mobile robots or unmanned ground vehicles. The laser ranging technique enables an accurate and robust measurement of the distance between an object and the sensor based on the time of flight principle. This work is aiming to develop a laser-based ranging system mounted on a planetary exploration rover. The basic requirement for such usage is the system to be small, lightweight, energy-efficient, and space-qualified. The system developed in this work is called Laser Range Imager (LRI), composed of the two-dimensional pixel arrays, the sensor processing unit, the laser diode and its driver, and the power distribution unit. This paper describes the development of the breadboard model for the LRI, along with its system overview and calibration techniques. The ranging performance of the LRI has been evaluated in field experiments.

1 Introduction

The planetary rover needs to traverse the surface of a planetary body with little knowledge of physical property of terrain. A high degree of autonomous mobility system enables the rover to evaluate terrain traversability in unknown/challenging environment and to navigate itself toward a location of interest. One of the key techniques of the autonomous mobility system is to measure a three dimensional terrain features around the rover and to access obstacle size, terrain slope angle, or terrain roughness. Visual information taken by an onboard stereoscopic camera have been counted on a promising approach for terrain assessment [1][2]. The visual information provides gray scale (or color) image data of the terrain but it may require a careful image calibration with a color palette, or the information may vary with the intensity of sunlight.

There has been extensive research and development in which the LIDAR (laser imaging detection and ranging) technique is used for sensing the environment and for classifying the terrain [3]. Several researches and developments have been reported, introducing the LIDAR technique for a possible application to the planetary rover [4][5][6]. A scanning-LIDAR system with gimbals has been widely used by unmanned ground vehicles, but its scanning mechanism may not be durable for launch/landing shocks or high vacuum lubrication in the space environment. Alternatively, a flash-LIDAR system that installs two-dimensional avalanche photodiode (APD) array can measure the distance of all objects in its field of view without any moving parts. While a space-qualified LIDAR has been used for a rendezvous and docking of the space shuttle to the international space station [7] as of 2012, there has been no actual rover that equips a LIDAR for its mission. A key issue of the flash LIDAR is related to the power consumption: it consumes relatively high energy (20–70 watts [8][9]) since the laser emission of the LIDAR needs to be strong enough as compared to the light intensity of background in order to achieve high signal to noise ratio in its measurement.

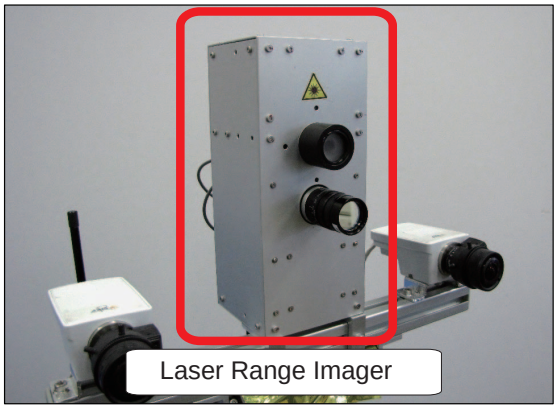

Figure 1. LRI prototype

The scope of this work is to develop a small-lightweight laser-based ranging system for the planetary exploration rover. The prototype developed in this work is called Laser Range Imager (LRI, Figure 1). The core technology of the LRI is the imaging device that detects the reflected light with timing-shifted dual gates. Each gate

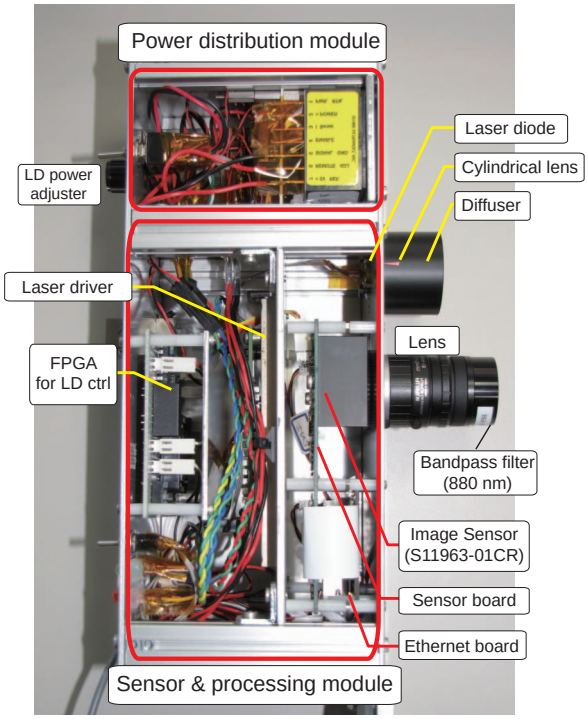

Figure 2. LRI componentss

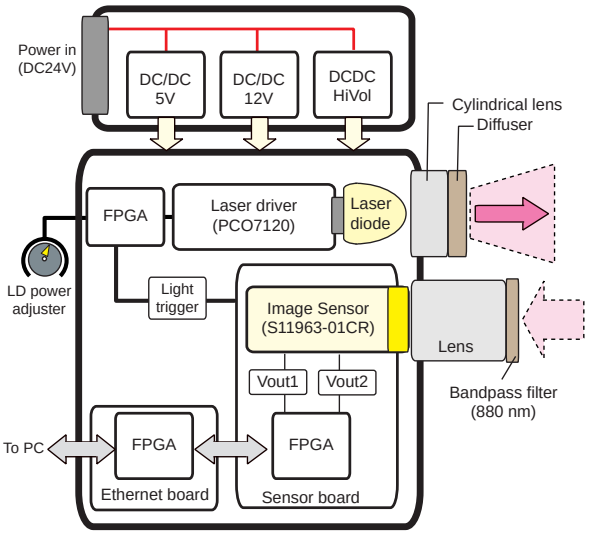

Figure 3. LRI schematic diagram

Table 1. LRI specification

Physical	
Mass	1.78 kg (incl. 0.95 kg of structure)
Dimension	94 × 100 × 234 mm
Power	5.5 W (max.)
Transmitting unit	
Laser	Pulsed laser diode L11348-330-04J
Power	90 W (max.)
Wave length	880 nm
Pulse width	30 ns
Receiving unit	
Sensor	S11963-01CR
Resolution	160 (W) × 120 (H)
Field of view	30 × 23 deg
Lens	HF9 HA-1B
Filter	λ_c=880 nm, Δ=12 nm

outputs a voltage proportional to the accumulated electric charges induced by the reflected light. The range information is then estimated from a ratio of the voltage provided from the two gates. This ranging principle needs a careful calibration with regard to a ranging error sensitivity as taking into account the intensity of the signal level. In this paper, the breadboard model of the LRI is described along with a calibration technique for an accurate ranging. The ranging performance of the LRI is evaluated in indoor/outdoor experiments.

The rest of this paper is organized as follows: Section 2 introduces the system overview of the LRI and Section 3 presents the ranging calibration technique. The field experiment for the LRI evaluation is described in Section 4.

2 Laser Range Imager

2.1 System overview

The LRI components and its schematic diagram are shown in Figure 2 and Figure 3, respectively. The specification of the LRI is summarized in Table 1.

The LRI consists of the sensor processing module and the power distribution module. The sensor processing module can be divided to the transmitting and receiving units. The pulsed laser emitted from the laser diode is expanded by the cylindrical lens such that the field of the light projection becomes 30 degrees in the horizontal and 23 degrees in the vertical. The laser light through the lens then passes the diffuser so that the ambiguity of the light intensity becomes relatively modest. The image sensor, S11963-01CR developed by Hamamatsu Photonics K.K., is the key device of the LRI which captures the light reflected from an object and accumulates the electric charges in timing-shifted dual gates. Voltages proportional to the accumulated electric charges from two gates, V_{out1} and V_{out2}, are then converted to the digital data and sent to a PC via the Ethernet board. The LD power adjuster is attached to the LRI prototype, for the purpose of failsafe for preventing an unexpected laser pulse emission with high-power/high-frequency.

The power distribution module provides regulated 5 VDC to the sensor/Ethernet boards, and also supplies both 12 VDC and high-voltage of 50 VDC to the laser driver.

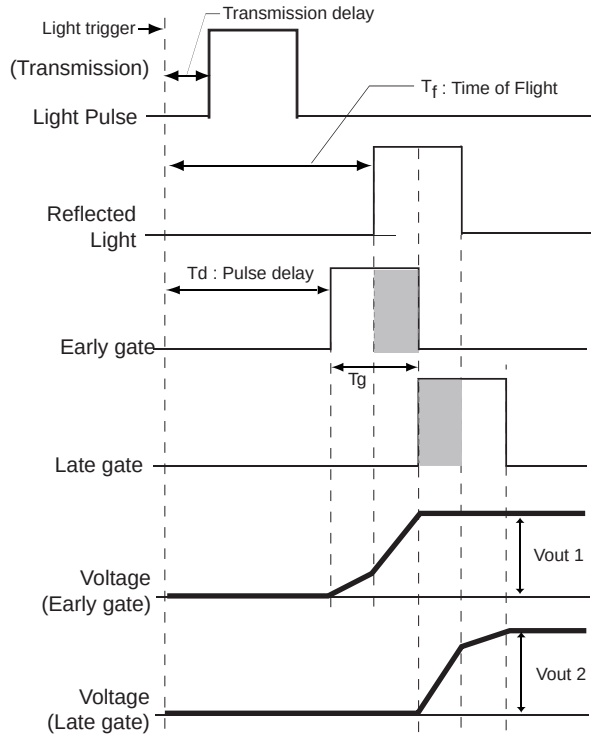

Figure 4. Timing chart based on the ranging principle

2.2 Ranging principle

The LRI has two gates similar to the early-gate/late-gate of a traditional mono-pulse radar technology [10]. It calculates the time difference of a reflected pulse with regard to the middle of two gate based on the difference of the amounts of the electric charges accumulated in the two gates.

Figure 4 shows a timing chart of the ranging principle of the LRI. First, the light pulse is emitted at a timing given from the image sensor (the light trigger as shown in Figure 3) with a transmisison delay and illuminates a scene. In practical, a jitter is observed in the light pulse profile, but its value is assumed as negligible in this work. The image sensor of the LRI then detects the light reflected from all the objects in the scene, with a time of flight T_f from the light emission. Here, each pixel of the image sensor array possesses two gates called as an early-gate and a late-gate. The early gate opens with a certain amount of delayed time (pulse delay, T_d) from the light trigger. The gate captures approximately first-half of the reflected light and then closes at a pre-determined gate width (T_g). Subsequently, the late gate opens and captures the last half of the reflected light within the width of T_g. The early and late gates charges capacitors during the gates are open. The image sensor reads out the voltages

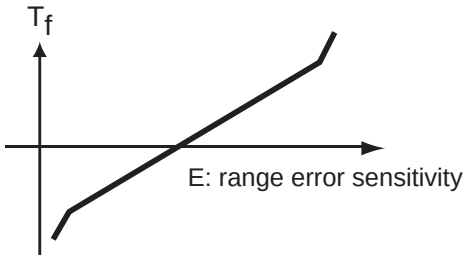

Figure 5. Range error sensitivity

(terms as V_{out1} and V_{out2}) that corresponds to the electric charges of the reflected light captured by each gate. In order to evaluate a ratio of the charges captured at both gates, the range error sensitivity E is defined as follows:

$$E = (V_{out1} - V_{out2})/(V_{out1} + V_{out2}) \quad (1)$$

It should be noted that V_{out1} and V_{out2} contain offset voltages due to the ambient light. Therefore, these offset voltages, or the dark level V_{dark1} and V_{dark2}, should be measured during the laser does not emit and be subtracted from V_{out1} and V_{out2}. Equation (1) is then rewritten using the voltages $V_1 = V_{out1} - V_{dark1}$ and $V_2 = V_{out2} - V_{dark2}$:

$$E = (\alpha V_1 - V_2)/(\alpha V_1 + V_2) \quad (2)$$

where α is the gate sensitivity ratio between the early and late gates.

The range error sensitivity is proportional to the time of flight T_f (Figure 5): $E = 0$ when the gates are properly centered with regard to the reflected light since the same amount of charges are captured; E becomes a negative value when the gates open earlier than the reflected light and E is positive when the gates opens later than that. Therefore the relationship of the range error sensitivity to the time of flight at each pixel coordinate (x, y) can be defined as follows:

$$T_f(x, y) = T_d - [a(x, y, S) \times E(x, y) + b(x, y, S)] \quad (3)$$

where a is a linearity coefficient and b is a time-offset coefficient, and S is the intensity of the reflected light and given by $(\alpha V1 + V2)/2$. The values of the coefficients a and b are determined from the range error calibration (see Section 3.2).

Finally, the distance D is calculated by the following equation:

$$D(x, y) = \frac{C}{2} \times T_f(x, y) + D_o(x, y) \quad (4)$$

where C is the velocity of light and D_o is the offset distance which is a distance used for the range error calibration. Applying the abovementioned technique to the output voltages from all the pixels, the range image is obtained.

Table 2. Typical values of the gate sensitivity ratio α

	Left (10)	Center (80)	Right (150)
Upper (10)	1.205	1.240	1.203
Middle (60)	1.194	1.206	1.173
Lower (110)	1.166	1.161	1.162

(The values in the parenthesis are the pixel coordinates)

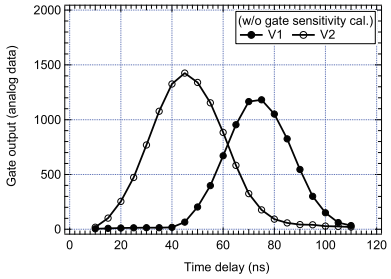

(a) w/o calibration

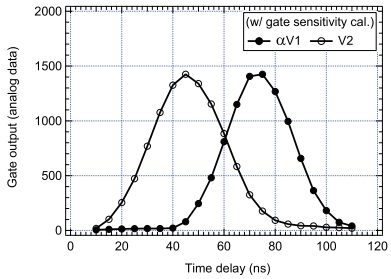

(b) w/ calibration

Figure 6. Gate sensitivity calibration of the center pixel

3 LRI Calibration Tests

3.1 Gate sensitivity calibration

The sensitivity with regard to the reflected light may not be equal between the early and late gates because of the sensor characteristics. In addition, the light pulse emitted from the laser diode and its reflected light do not form square waves as shown in Figure 4 but they forms like asymmetric V-shape waves. Therefore, the charges captured at the both gates will not be equal even if the gates are properly centered with regard to the reflected light. In this work, this difference due to the irregular light pulse shape is also compensated by the gate sensitivity ratio.

The gate sensitivity calibration is performed to identify the value of the parameter α in Equation (2). In the calibration test, the LRI is fixed in front of a white flock paper with a distance of 1.0 m. Then, the output voltages V_1 and V_2 are measured with varying the pulse delay T_d from 10 ns to 110 ns with the step of 5 ns. The gate width T_g is set as 30 ns.

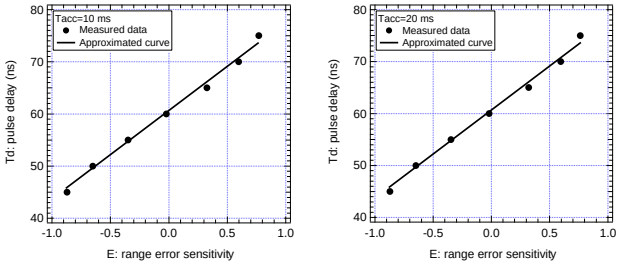

(a) T_{acc} = 10 ms (b) T_{acc} = 20 ms

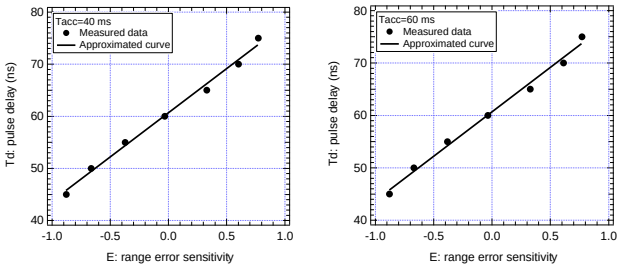

(c) T_{acc} = 40 ms (d) T_{acc} = 60 ms

Figure 7. Range error sensitivity measuread from the calibration (center pixel)

The sensitivity ratio is calculated by comparing the peak values of both voltage curves (Figure 6a):

$$\alpha(x,\ y) = \max(V_2(x,\ y))/\max(V_1(x,\ y)) \qquad (5)$$

Figure 6b shows the calibrated curves of the output voltages of the center pixel. Table 2 summarizes typical values of α in the upper/middle/lower and the left/center/right pixels. From the above calibration, the average value of the gate sensitivity is 1.198 ± 0.026 (1σ).

3.2 Range error calibration

The range error calibration is related to the determination of the coefficients a and b in Equation (3).

In the calibration test, the LRI is fixed in front of a white flock paper with a distance of 1.0 m. The output voltages V_1 and V_2 are measured with varying the pulse delay T_d from 40 ns to 80 ns with the step of 5 ns. Note that V_1 and V_2 have almost same voltages when T_d = 60 ns. The integration time* T_{acc} varies from 10 ms to 80 ms in order to change the intensity of the reflected light. The gate width T_g is set as 30 ns.

Figure 7 shows the relationship between the pulse delay and the range error sensitivity of the center pixel measured at the calibration tests. It can be seen that the curves are linearly approximated in the range of T_d [50 ns, 70

*T_{acc} is equivalent to a shutter speed of a still camera: larger T_{acc} provides higher intensity.

Table 3. Coefficients determined by the range error calibration (center pixel)

T_{acc} (ms)	a (ns)	b (ns)	R^2 (%)	S (count)
10	15.77	60.31	99.87	728.5
20	15.84	60.32	99.90	1463.5
40	15.45	60.42	99.81	3031.9
60	15.25	60.44	99.82	4643.2
Mean	15.58	60.37	N/A	N/A
Std.	0.277	0.067	N/A	N/A

Table 4. LRI calibration statistics: ranging error averaged from the entire pixels. (the unit is in meters)

	T_d (ns)				
T_{acc} (ms)	50	55	60	65	70
10	0.036	0.006	0.014	0.061	0.045
20	0.050	0.005	0.007	0.047	0.060
40	0.005	0.048	0.014	0.069	0.041
60	0.019	0.105	0.041	0.085	0.004

ns]. The coefficients a and b for Equation (3) and the coefficient of determination R^2 are summarized in Table 3. The linear regression accurately approximates the measured values. In other words, the range error calibration between T_d [50 ns, 70 ns] calculated here shows high confidence for its approximation. The linear approximation in this paper was performed in the range of Δ20 ns centering around T_d = 60 ns. This indicates that the linearity is assured within ±10 ns ≡ ± 1.5 m under a fixed value of T_d. For an accurate ranging, T_d should be preliminarily tuned in accordance with a target to be measured such that the early and late gates provide almost same voltages.

The coefficients a and b given from the calibration are relatively constant relative to the intensity as summarized in Table 3. The standard deviation of a is 0.277 ns which will cause an error of ± 0.041 m while that of b is 0.067 ns, or ± 0.010 m. These coefficients are then assumed as the intensity-invariant in this case, and therefore, the average value between them are used in the following tests. These errors are considered as the ranging accuracy of the LRI determined from the calibration. It should be noted that they may need to be approximated as a function of the intensity if the values of the coefficients significantly increase/decrease as the intensity.

3.3 LRI calibration statistics

The LRI calibration performance can be evaluated by the following scenario: the LRI is fixed in front of a white flock paper with a distance of 1.0 m, and measures the output voltages with varying T_d and T_{acc}. Subsequently, the time of flight T_f is calculated from Equation (3) using the coefficients determined by the abovementioned calibrations (α, a, and b), and then, the distance is given from Equation (4). Here, the distance offset D_o is 1.0 m that was the distance having been used in the range error calibration. This post-process evaluates how accurate the ranging principle used in this work can correlate with the practical ranging.

Table 4 shows the LRI calibration performance in terms of the ranging error with regard to the true value of 1.0 m. The value in each cell of the table is the average value between the ranging errors of the entire pixels. From the table, it can be summarized that the average ranging error is about 0.038 m ± 0.029 m (1σ). These errors are generated by the linear approximation error as discussed in Table 3.

4 LRI Ranging Tests

4.1 Indoor tests (target: color palette)

The ranging performance of the LRI was preliminarily evaluated at indoor experiment under a constant ambient light. In this test, the LRI was fixed such that it directed to two color palettes on a white flock paper: one of them, the 3-color palette includes the white, gray, and black (Figure 8) while the other is the 9-color palette having RGB (red, green, and blue), CMY (cyan, magenta, and yellow), and the grayscale (Figure 9). The distance between the palette and the LRI was 1.0 m for the 3-color palette, and 2.26 m/3.15 m for the 9-color palette. The pulse delay T_d is tuned such that the gates are centered with regard to the reflected light.

Figure 8 shows the range image and corresponding intensity data. The range data could not be calculated at the area colored by black because the intensity reflected from that area is too small to reproduce the ranging data. The other areas colored by the white and the gray were successfully measured. The ranging results for the 9-color palette are depicted in Figure 9. In the both distances, the area colored by black could not be detected because of its less intensity of the reflected light. Also, the range of the gray region in the case of 3.15 m was estimated a bit shorter than the true value. This is also due to the less reflection of the light, causing less accuracy of its ranging. Other than these areas, the LRI successfully measured the color palettes as those distances were almost equivalent to the distance of the background white flock paper.

The statistics of the ranging tests are summarized in Table 5. D_{ave} is the average ranging value between the entire pixels. From the table, it is confirmed that the LRI has a ranging performance with an accuracy of less than 0.08 m.

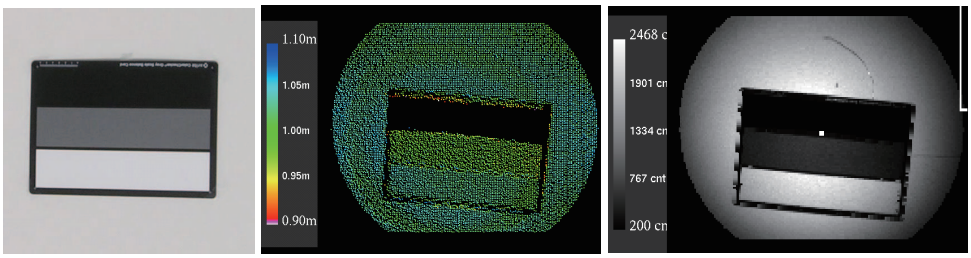

3-color palette | Range image | Intensity image

Figure 8. LRI ranging test for 3-color palette

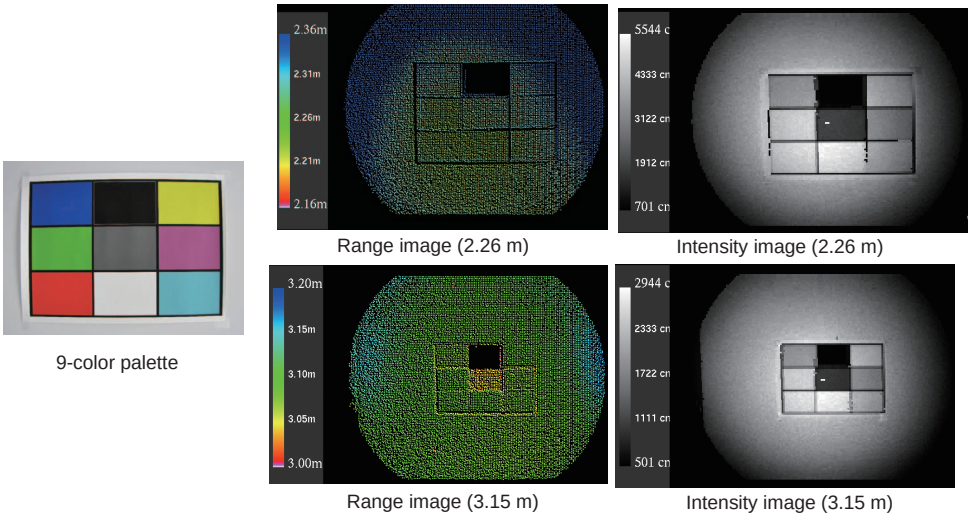

9-color palette

Range image (2.26 m) | Intensity image (2.26 m)

Range image (3.15 m) | Intensity image (3.15 m)

Figure 9. LRI ranging test for 9-color palette

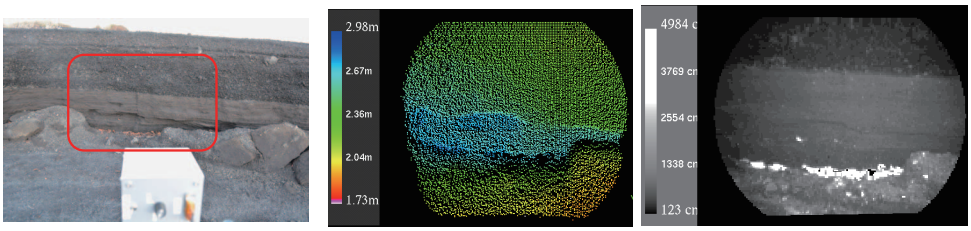

Overview of the measurement | Range image | Intensity image

Figure 10. LRI field testing: geological layer of a gully erosion

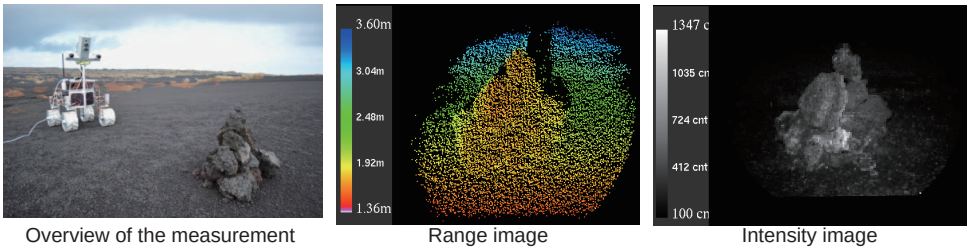

Overview of the measurement | Range image | Intensity image

Figure 11. LRI field testing: accumulated rocks

Table 5. LRI ranging statistics (target: color palette)

Target (m)	T_d (ns)	D_{ave} (m)	Error (m)	D_{std} (m)
1.00	60	1.02	0.02	0.02
2.26	60	2.30	0.04	0.05
	65	2.33	0.07	0.05
	70	2.20	-0.06	0.02
3.15	65	3.07	-0.08	0.03
	70	3.10	-0.05	0.02
	75	3.08	-0.07	0.03

4.2 Field testing

A field demonstration of the LRI was also performed at a volcanic area, where the terrain is mostly covered with basalt/scoria. Such materials have very low reflection ratio (less than 5 %). Therefore, the integration time T_{acc} was set as relatively large value (600–1200 ms) in order to capture the reflected light sufficient for the ranging.

Figure 10 shows the range/intensity images of a geological layer of a gully erosion. The intensity image illustrates the varied intensity of the light reflected from different geological layer of the terrain, and the range image also depicts the three-dimensional feature of the erosion. The true value of the distance between the LRI to the area where the center pixel collimated was 2.70 m while that measured by the LRI was 2.50 m with T_d=70 ns and T_{acc}=1200 ms. Figure 11 was the result for the ranging of an accumulated rocks (T_d=65 ns and T_{acc}=800 ms). The shape of the aggregate was successfully captured as seen in the range image. The error between the true distance and the distance measured by the LRI was about 0.20 m. This error may be caused by the following reason: the low reflection ratio of the terrain requires longer integration time that also increased a chance of the disturbance from a varying ambient light in the test field.

The field testing reveals that the LRI achieved to qualitatively measure several objects in the outdoor condition, but an additional calibration technique related to the intensity data would be applied for more accurate ranging.

5 Conclusions and Future Works

This paper has described the development of the LRI breadboard model that achieves low power with high frame rate, being capable of measuring the distance with an accuracy of less than 0.08 m in the indoor test. The ranging principle of the LRI is based on the timing-shifted dual gates: the early-gate/late-gate principle used for a traditional mono-pulse radar technology. The LRI calibration in this work has focused on the gate sensitivity and the range error sensitivity, and further calibration such as an intensity-dependent calibration will be required for more accurate ranging for outdoor usage. The components used for the LRI are commercially available, and therefore, environmental testings should be required for further development towards a space-qualified LRI.

Acknowledgment

The authors would like to acknowledge Ariya Sunako, Jun Hiramitsu, Takashi Suzuki, Mitsuhito Mase, and Shigeyuki Nakamura of Hamamatsu Photonics K.K, for providing the image sensor and their technical advises in the development of the LRI.

References

[1] Maimone, M., Johnson, A., and Cheng, Y., "Autonomous Navigation Results from the Mars Exploration Rover (MER) Mission," Proc. of the 9th Int. Symp. on Experimental Robotics, Singapore, pp. 3–13, 2004.

[2] Matthies, L., Maimone, M., Johnson, A., Cheng, Y., Willson, R., Villalpando, C., Goldberg, S., and Huertas, A., "Computer Vision on Mars," Int. Journal of Computer Vision, Vol. 75, No. 1, pp. 67–92, 2007.

[3] Buehler, M., Iagnemma, K., and Singh, S., (eds), The DARPA Urban Challenge: Autonomous Vehicles in City Traffic, Springer Tracts in Advanced Robotics (STAR) Series, Vol. 56. Springer-Verlag Berlin Heidelberg, 2009.

[4] Vaskevicius, N., Birk, A., Pathak, K., and Schwertfeger, S., "Efficient Representation in 3D Environment Modeling for Planetary Robotic Exploration," Advanced Robotics, vol. 24, no. 8–9, pp.1169–1197, 2010.

[5] Dong, H., and Barfoot. T., "Lighting-Invariant Visual Odometry using Lidar Intensity Imagery and Pose Interpolation," Proc. of the 8th Int. Conf. on Field and Service Robotics, July, 2012.

[6] Bakambu, J., Nimelman, M., Tripp, J., and Kujelev, A., "Compact Fast Scanning Lidar for Planetary Rover Navigation," Proc. of the Int. Symp. on Artificial Intelligence, Robotics and Automation in Space 2012.

[7] Luu, T., Ruel, S., and Berube, A., "TriDAR Test Results Onboard Final Shuttle Mission, Applications for Future Of Non-Cooperative Autonomous Rendezvous & Docking," Proc. of the Int. Symp. on Artificial Intelligence, Robotics and Automation in Space 2012.

[8] "SR4500," MESA Imaging AG, http://www.mesa-imaging.ch/products/sr4500/ , Retrieved Apr. 15th, 2014.

[9] "DragonEye 3D Flash LIDAR Space Camera," Advanced Scientific Concepts, Inc., http://www.advancedscientificconcepts.com/products /dragoneye.html , Retrieved Apr. 15th, 2014.

[10] Skolnik, M., *Radar Handbook*, McGraw-Hill, Inc., 1970.